# COVID-19 PANDEMIC REVEALS PERSISTENT DISPARITIES IN NITROGEN DIOXIDE POLLUTION

GAIGE HUNTER KERR[1], DANIEL L. GOLDBERG[1,2], SUSAN C. ANENBERG[1]

[1]*Department of Environmental and Occupational Health, Milken Institute School of Public Health, George Washington University, Washington, DC, 20052 USA,* [2] *Energy Systems Division, Argonne National Laboratory, Lemont, IL, 60439 USA*

## 1. Abstract

The unequal spatial distribution of ambient nitrogen dioxide ($NO_2$), an air pollutant related to traffic, leads to higher exposure for minority and low socioeconomic status communities. We exploit the unprecedented drop in urban activity during the COVID-19 pandemic and use high-resolution, remotely-sensed $NO_2$ observations to investigate disparities in $NO_2$ levels across different demographic subgroups in the United States. We show that prior to the pandemic, satellite-observed $NO_2$ levels in the least white census tracts of the United States were nearly triple $NO_2$ levels in the most white tracts. During the pandemic, the largest lockdown-related $NO_2$ reductions occurred in urban neighborhoods that have 2.0 times more non-white residents and 2.1 times more Hispanic residents than neighborhoods with the smallest reductions. $NO_2$ reductions were likely driven by the greater density of highways and interstates in these racially and ethnically diverse areas. Although the largest reductions occurred in marginalized areas, the effect of lockdowns on racial, ethnic, and socioeconomic $NO_2$ disparities was mixed and, for many cities, non-significant. For example, the least white tracts still experienced $\sim 1.5$ times higher $NO_2$ levels during the lockdowns than the most white tracts experienced prior to the pandemic. Future policies aimed at eliminating pollution disparities will need to look beyond reducing emissions from only passenger traffic and also consider other collocated sources of emissions such as heavy-duty trucks, power plants, and industrial facilities.

*E-mail address*: gaigekerr@gwu.edu.

## 2. Significance Statement

We leverage the unparalleled changes in human activity during COVID-19 and the unmatched capabilities of the TROPOspheric Monitoring Instrument to understand how lockdowns impact ambient nitrogen dioxide ($NO_2$) pollution disparities in the United States. The least white communities experienced the largest $NO_2$ reductions during lockdowns; however, disparities between the least and most white communities are so large that the least white communities still faced higher $NO_2$ levels during lockdowns than the most white communities experienced prior to lockdowns despite a $\sim 50\%$ reduction in passenger vehicle traffic. Similar findings hold for ethnic, income, and educational attainment subgroups. Future strategies to reduce $NO_2$ disparities will need to target emissions from not only passenger vehicles but other collocated on-road and stationary sources.

## 3. Introduction

Adverse air quality is an environmental justice issue as it disproportionately affects marginalized and disenfranchised populations around the world [Bell and Ebisu, 2012, Landrigan et al., 2018, Schell et al., 2020, Demetillo et al., 2020]. Growing evidence suggests that these populations experience more air pollution than is caused by their consumption [Nguyen and Marshall, 2018, Tessum et al., 2019, Sergi et al., 2020]. Within the United States (U.S.), disparities in exposure are persistent, despite successful regulatory measures that have reduced pollution [Clark et al., 2017, Colmer et al., 2020]. Nitrogen dioxide ($NO_2$) is a short-lived trace gas formed shortly after fossil fuel combustion and regulated by the National Ambient Air Quality Standards under the Clean Air Act. Exposure to $NO_2$ is associated with a range of respiratory diseases and premature mortality [Jerrett et al., 2013, Anenberg et al., 2018, Achakulwisut et al., 2019]. $NO_2$ is also a precursor to other pollutants such as ozone and particulate matter [Stohl et al., 2015]. Major sources of anthropogenic $NO_2$, such as roadways and industrial facilities, are often located within or nearby marginalized and disenfranchised communities [Mohai et al., 2009, Rowangould, 2013], and disparities in $NO_2$ exposure across demographic subgroups have been the focus of several recent studies [Hajat et al., 2013, Clark et al., 2014, Clark et al., 2017, Demetillo et al., 2020].

In early 2020, governments around the world imposed lockdowns and shelter-in-place orders in response to the spread of the coronavirus disease 2019 (COVID-19). The earliest government-mandated lockdowns in the U.S. began in California on 19 March 2020, and many states followed suit in the following days. Changes in mobility patterns indicate that self-imposed social distancing practices were underway days to weeks before the formal announcement of lockdowns [Badr et al., 2020]. Lockdowns led to sharp reductions in surface-level $NO_2$ [He et al., 2020, Parker et al., 2020, Shi and Brasseur, 2020, Venter et al., 2020] and tropospheric column $NO_2$ measured from satellite instruments [Bauwens et al., 2020, Ding et al., 2020, Goldberg et al., 2020, Miyazaki et al., 2020, Parker et al., 2020] over the U.S., China, and Europe. According to government-reported inventories, roughly 60% of anthropogenic emissions of nitrogen oxides ($NO_x \equiv NO + NO_2$) in the U.S. in 2010 were emitted by on-road vehicles [US Environmental Protection Agency, 2015], and up to 80% of ambient $NO_2$ in urban areas can be linked to traffic emissions [Levy et al., 2014, Sundvor et al., 2013]. As such, $NO_2$ is often used as a marker for road traffic in urban areas. Multiple lines of evidence such as seismic quieting and reduced mobility via location-based services point to changes in traffic-related emissions as the main driver of reductions in $NO_2$ pollution during lockdowns due to the large proportion of the population working from home [Diffenbaugh et al., 2020, Lecocq et al., 2020, Venter et al., 2020].

Here we exploit the unprecedented changes in human activity unique to the COVID-19 lockdowns and remotely-sensed $NO_2$ columns with unprecedented spatial resolution and coverage to understand inequalities in the distribution of $NO_2$ pollution for different racial, ethnic, and socioeconomic subgroups in the U.S. Specifically, we address the following: Which demographic subgroups received the largest $NO_2$ reductions? Did the lockdowns grow or shrink the perennial disparities in $NO_2$ pollution across different demographic subgroups? Although the lockdowns are economically unsustainable, how can they advance environmental justice and equity by informing long-term policies to reduce $NO_2$ disparities and the associated public health damages?

## 4. Results

Previous studies examining satellite-derived $NO_2$ found the highest levels in urban areas [Krotkov et al., 2016, Cooper et al., 2020, Goldberg et al., 2021], and we find that these areas clearly stand out as $NO_2$ hotspots during our baseline period (Figure 1a). $NO_2$ column densities averaged over all urban areas are $\sim 2$ times higher than over rural areas during the baseline period. Absolute differences in $NO_2$ between the baseline and lockdown periods ("drops") show sharp decreases over virtually all major metropolitan regions (Figure 1b). The use of only spring 2019 for our baseline period stems from the short data record offered by TROPOMI, and the slight increases in $NO_2$ in parts of the Great Plains and Midwest during lockdowns ($< 0.5 \times 10^{15}$ molecules cm$^{-2}$) could reflect differences in natural (e.g., soil, lightning, stratospheric $NO_x$) or anthropogenic sources of $NO_2$ between the baseline and lockdown periods. We use 3 month periods for our baseline and lockdown periods in lieu of a shorter timeframe in order to account of daily, weekly, and monthly fluctuations in meteorology. Given that the largest lockdown-related changes in $NO_2$ occur in urban areas and to avoid urban-rural demographic gradients, we primarily focus on urban $NO_2$ changes and how these changes impact different demographic subgroups in urban areas.

The largest urban $NO_2$ drops occur in census tracts that are more non-white and Hispanic, have lower median household income, and have a higher proportion of

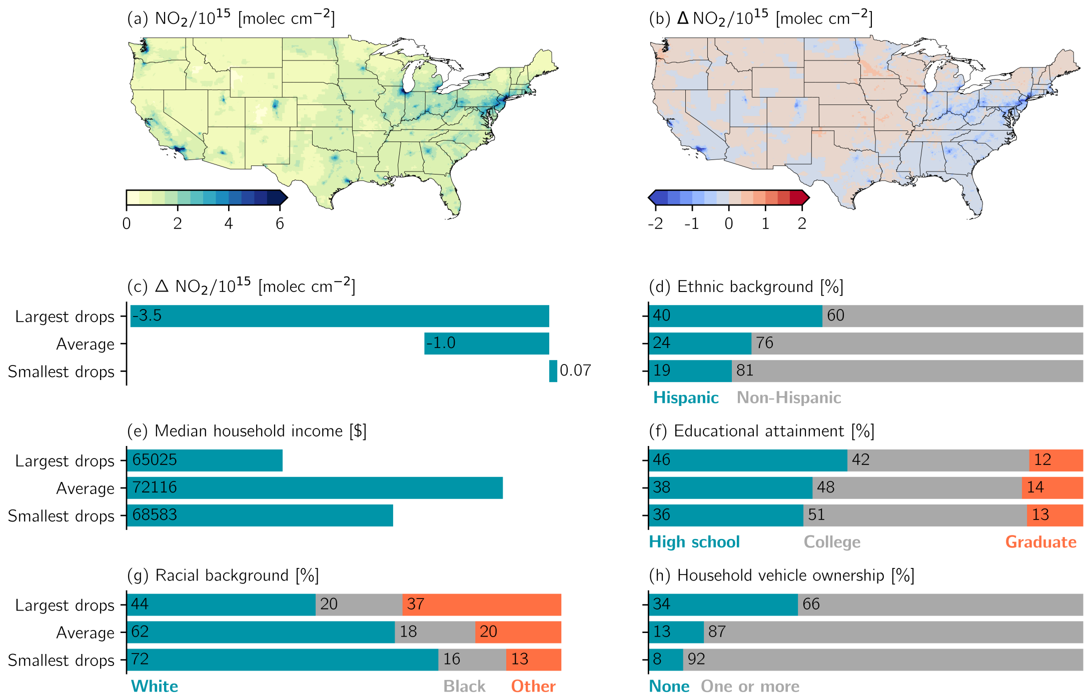


FIGURE 1. **Spatial distribution of $NO_2$ columns during the baseline and COVID-19 lockdown periods and apportionment of drops among different demographic subgroups.** (a) Census-tract average baseline $NO_2$ (13 March-13 June 2019). (b) Absolute difference between lockdown (13 March - 13 June 2020) and baseline $NO_2$ ($\Delta$ $NO_2$), where $\Delta$ $NO_2 < 0$ corresponds to $NO_2$ drops during lockdowns. (c-h) Demographic data averaged over urban tracts with the largest drops ($\Delta$ $NO_2$ in first decile), all urban tracts, and urban tracts with the smallest drops ($\Delta$ $NO_2$ in the tenth decile). "Other" in (g) includes American Indian or Alaska Native, Asian, Native Hawaiian or other Pacific Islander, two or more races, and some other race. The census-designated concept of race differs from ethnicity, and the percentage of white residents in (g) includes individuals with Hispanic origin or descent.

their population without a vehicle or a post-secondary education compared with tracts with the smallest drops (Figure 1d-h). In tracts with the largest drops, there are $\sim$ 2.0 times more non-white residents and $\sim$ 2.1 times more Hispanic residents than in tracts with the smallest drops (Figure 1d, g). The differences in the "Other" category between tracts with largest and smallest drops (Figure 1g) reflects differences in the Asian population (5% in tracts with the smallest drops; 14% in tracts with the largest drops) and the proportion of the population who does not identify as one of the census-designed racial categories (4% in tracts with smallest drops; 19% in tracts with the largest drops). These results for urban tracts also hold in all (urban and rural) tracts and rural tracts, despite the different demographic composition of the population for these conglomerations (compare Figures 1 and S1). Differences in distributions of demographic variables between tracts with the largest versus smallest drops in Figure 1c-h are all statistically significant.

Communities with lower income and educational attainment and a large proportion of racial and ethnic minorities have faced higher levels of $NO_2$ and other pollutants for decades [Hajat et al., 2013, Hajat et al., 2015, Clark et al., 2017, Colmer et al., 2020, Schell et al., 2020], and we find that these communities experienced the largest drops in $NO_2$ pollution during COVID-19 lockdowns. However, Figure 1 does not indicate how lockdown-related $NO_2$ drops grew or shrunk disparities, and we next examine disparities in baseline and lockdown $NO_2$ in the most marginalized versus least marginalized census tracts in the U.S.

In the baseline and lockdown periods, neighborhoods with lower income and educational attainment and those with a higher proportion of minority residents consistently face higher levels of $NO_2$ among all urban tracts across the U.S. and in nearly all of the 15 largest metropolitan statistical areas (MSAs) in the U.S. (Figures 2, S2). Rural tracts with the *highest* income and educational attainment, however, have *higher* $NO_2$ levels than tracts with the lowest income or educational attainment (Figure 2b-c), and similar findings hold for specific MSAs (e.g., Riverside in Figure 2b, Atlanta in Figure 2c). Moreover, there are no significant differences in $NO_2$ distributions for tracts with the highest versus lowest income during the baseline period (Figure 2a).

When considering all census tracts (both urban and rural), the most pronounced disparities, defined as the ratio of mean $NO_2$ for the marginalized subgroup to the non-marginalized subgroup, are on the basis of race and ethnicity. The least white tracts and most Hispanic tracts have 2.6 and 2.2 times greater baseline $NO_2$ levels than the most white and least Hispanic tracts, respectively (Figures 2a, S2a, S3g). These disparities persist when examining the individual MSAs in the U.S. For example, baseline $NO_2$ in tracts with the lowest median household income in New York and Los Angeles is 1.4 and 1.8 times higher, respectively, than tracts with the highest income (Figures 2b, S2b).

The unprecedented change in human activity during COVID-19 lockdowns led to mixed impacts on relative $NO_2$ disparities across different population subgroups, depending on the demographic variable and MSA considered (Figures 2, S2). Racial $NO_2$ disparities for all census tracts significantly decreased from 2.6 to 2.0 during lockdowns, and a majority of the featured MSAs experienced significant reductions in their racial disparities (Figures 2a, S2a). Disparities for other demographic variables, however, were less affected by lockdowns. For example, a majority of MSAs had no significant reduction in disparities for different levels of income and educational attainment (Figures 2b-c, S2b-c).

Although urban areas experienced broad drops in $NO_2$ during lockdowns with the largest drops occurring in marginalized neighborhoods (Figure 1c-h), $NO_2$ disparities in the baseline period were so large that even significant reductions in disparities did not generally bring lockdown $NO_2$ levels for marginalized neighborhoods to the levels experienced by non-marginalized neighborhoods during the baseline period (Figures 2, S2). As an example: despite the unprecedented drop in human activity during the COVID-19 pandemic, $NO_2$ levels in the least white neighborhoods in New York and Chicago were $\sim 1 \times 10^{15}$ and $\sim 2 \times 10^{15}$ molecules cm$^{-2}$ higher, respectively, during lockdowns than levels in the most white neighborhoods during the baseline period. Houston, Washington, Philadelphia, and San Francisco are notable exceptions to this result, and $NO_2$ levels for the least white tracts during lockdowns fell below $NO_2$ levels for the most white tracts during the baseline period in these cities. We observe similar results for population subgroups based on ethnicity, income, and educational attainment (Figures 2, S2).

Within urban areas, we find that the magnitude of $NO_2$ drops is tightly coupled to the density of nearby primary roads (highways and interstates). The density of primary roads in urban tracts with the largest $NO_2$ drops (i.e., tracts in the first decile) is $\sim$ 9.5 times greater than in urban tracts with the smallest $NO_2$ drops (i.e., tenth decile) (Figure 3). The racial, ethnic, income, and educational composition of tracts are also closely related to primary road density; urban tracts with lower income and vehicle ownership and a larger percentage of racial and ethnic minorities are located near a higher density of primary roads (Figure 3). The difference in primary road density on the basis of vehicle ownership is especially stark: tracts with the lowest vehicle ownership have a $\sim$ 9.5 times higher primary road density than tracts with the highest ownership. Similarly, the least white tracts have a primary road density $\sim$ 4.5 times higher than the most white tracts. Educational attainment is the only demographic variable considered in this study that exhibits a different relationship with primary road density, and we observe a U-shaped relationship between these variables (Figure 3).

To better understand the impact of the lockdowns on $NO_2$ exposure disparities, we consider case studies of individual cities: New York, Detroit, and Atlanta (Figure 4). Among individual neighborhoods in each of these cities, the magnitude of $NO_2$ drops vary up to 50% above and below the citywide average (Figure 4a-c). The portions of New York, Atlanta, and Detroit that received the largest drops tend to have lower median household income and a high percentage of non-white residents (Figure 4d-i). In New York the largest drops are concentrated in Harlem and The South Bronx (Figure 4a), where the high concentration of major highways and industrial facilities has been linked to disproportionate exposure to air pollution [Patel et al., 2009]. The largest drops in Atlanta occur in the southwestern part of the city where median household income generally is $<$ \$30000 and

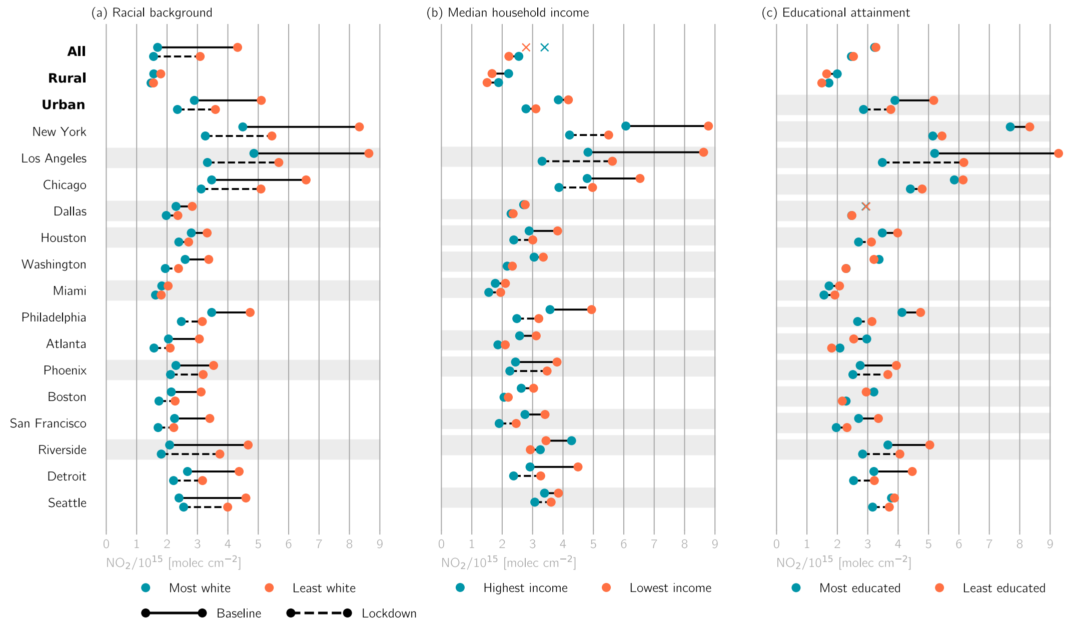


FIGURE 2. **Disparities in baseline and lockdown $NO_2$ columns across different demographic subgroups.** Disparities are shown for three conglomerations (all, urban, and rural census tracts), and urban tracts are further separated into the fifteen largest MSAs in the U.S. For each conglomeration or MSA, demographic subgroups are determined using the 10th and 90th percentiles as thresholds. $NO_2$ levels are thereafter averaged over tracts within these subgroups. If the difference in subgroup $NO_2$ distributions for a particular demographic variable and time period is not statistically significant, mean $NO_2$ levels are denoted with an "X" and no connector lines. Conglomerations or MSAs with no significant change in $NO_2$ disparities between the baseline and lockdown periods are shaded in grey.

the percentage of Black residents in each tract is nearly 100. Although large-scale drops in $NO_2$ are primarily driven by reductions in on-road emissions [Quéré et al., 2020, Venter et al., 2020], examining drops on smaller spatial scales, such as in Atlanta (Figure 4b), suggests that emissions from other sectors may be at play. In Atlanta, the largest drops occur southwest of downtown, near Hartsfield-Jackson International Airport and several major highways (Figure 4b). The airport reported a $\sim$ 50% decrease in the daily number of flights during lockdowns [Shah, 2020]. Therefore, both on-road and aviation emissions may be responsible for the disparities in $NO_2$ levels in Atlanta. The largest drops in Detroit are concentrated on the west shores of the Detroit River; Interstates 75 and 94 and the Ambassador

Bridge, one of the busiest U.S.-Canada border crossing, transect this part of Detroit (Figure 4c) [Martenies et al., 2017]. Although these Detroit neighborhoods are not predominantly non-white (Figure 4f), they are home to a large Hispanic population (not shown) with low median household income (Figure 4i).

## 5. Discussion

Neighborhoods with a large population of racial and ethnic minorities, lower income, and lower educational attainment saw improvements in $NO_2$ pollution during the COVID-19 lockdowns. Although lockdowns were lauded as a temporary glimpse of the potential for cleaner urban air, $NO_2$ disparities persisted during this global natural experiment. For many cities, there were no significant changes in $NO_2$ disparities during the lockdowns, and marginalized communities faced higher $NO_2$ levels during the lockdowns than non-marginalized communities experienced prior to the lockdowns. Overall, these findings are consistent with contemporaneous studies that have analyzed long-term trends in $NO_2$ and other air pollutants and found that, despite widespread decreases in pollution, the most exposed demographic subgroups in the 1980s and 1990s remain the most exposed in the present-day [Clark et al., 2017, Colmer et al., 2020].

Tracts' proximities to roadways may be responsible for both the lockdown-related drops and the persistent disparities of $NO_2$ pollution among demographic subgroups (Figures 1-3). The collocation of primary roads with poor, minority communities is not happenstance but a consequence of the Eisenhower-era federal highway program, which often deliberately routed highways through these poor, minority neighborhoods [Rose and Mohl, 2012, Boehmer et al., 2013, Rowangould, 2013, Clark et al., 2017]. Additionally, other potent sources of pollution such as power plants, manufacturing facilities, and heavy-duty trucking operations are also collocated with primary roads due to these industries' needs for highway access [Mohai et al., 2009, Demetillo et al., 2020].

Interestingly, urban tracts with the lowest vehicle ownership have both the highest density of nearby primary roads and the largest drops in $NO_2$ (Figures 1h, 3). This result suggests that these communities may breathe more traffic-related $NO_2$ pollution than they produce. This is indeed the case for particulate matter pollution: recent work found that particulate matter exposure is disproportionately caused by rich, non-Hispanic white communities, while poor, Black and Hispanic communities face higher exposure than is caused by their own consumption [Tessum et al., 2019, Sergi et al., 2020].

Preliminary research suggests that high levels of $NO_2$ pollution contribute to underlying health conditions that lead to increased COVID-19 fatality rates [Liang et al., 2020]. Therefore, the decrease in $NO_2$ in diverse communities with low income or educational attainment (Figure 2) could decrease population susceptibility to COVID-19. This result is especially important as these communities have

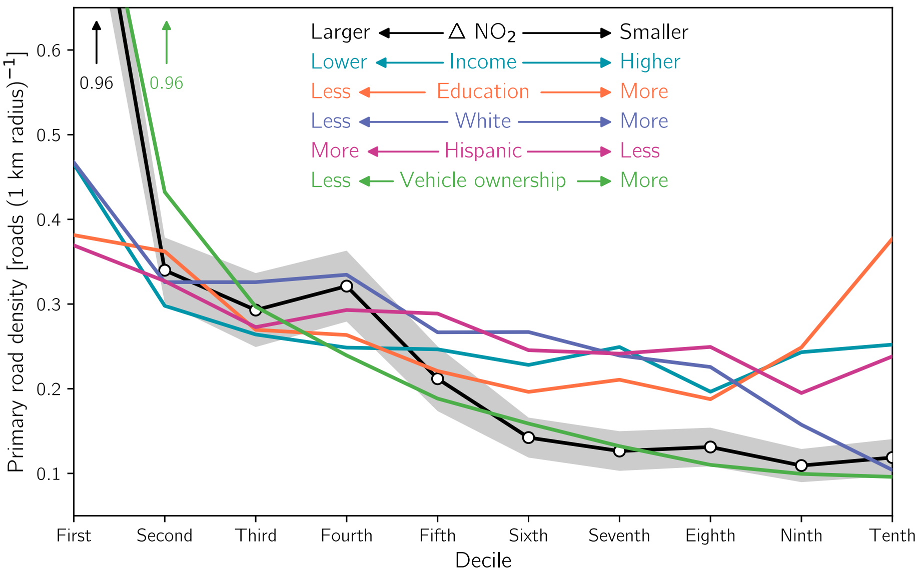


FIGURE 3. **The relationship of road density with urban lockdown-related drops in $NO_2$ columns and demographic variables.** Road density is calculated as the number of primary road segments within a 1 km radius of tracts' centroids for each decile of demographic variables. The colored legend indicates the directionality of each demographic variable. As an example, the density corresponding to the lowest decile of the "White" curve represents the road density in urban tracts that are the least white (i.e. in the first decile of the percentage of their population that is white). Shading for the $\Delta NO_2$ curve illustrate the 90% confidence interval.

increased risk to COVID-19 and higher hospitalization rates [Raifman and Raifman, 2020]. Since short-term $NO_2$ exposure is associated with respiratory disease [Chauhan et al., 2003, Hansel et al., 2015], the temporary $NO_2$ drops may have also reduced acute respiratory health outcomes, but the actual health effects of $NO_2$ drops during the pandemic are difficult to tease out since the degree to which people sought health care was also affected by the pandemic. These findings are especially relevant for marginalized neighborhoods in cities (e.g., New York, Atlanta, and Detroit; Figure 4) that have been long-plagued by high rates of asthma and other respiratory diseases due, in part, to their proximity to on-road and point source $NO_x$ emissions [Patel et al., 2009, Martenies et al., 2017].

We have considered singular demographic variables and their relationship with baseline and lockdown $NO_2$. The case studies in Figure 4 hint that the intersectionality between race and poverty may be associated with even more pronounced lockdown-related drops in $NO_2$ pollution. Although the vast majority of tracts in the southern half of Atlanta have a majority non-white population (Figure 4h), the largest drops occur in tracts that are both majority non-white and low income (Figure 4b, e, h). Clark et al. [Clark et al., 2014] and Demetillo et al. [Demetillo et al., 2020] examined $NO_2$ exposure in neighborhoods where poverty and racial and ethnic identities intersect and found a disproportionate share of $NO_2$ pollution for neighborhoods with these intersecting identities. Assessing other forms of intersectionality and their relationship with air pollution exposure is a key area for future research.

Recent work demonstrates that satellite-observed $NO_2$ is a powerful proxy for ground-level $NO_2$ gradients [Bechle et al., 2013], and TROPOMI, in particular, provides significant advances over predecessor instruments on account of its unprecedented spatial resolution [Goldberg et al., 2019]. We tested whether TROPOMI has consistent spatial patterns with surface-level observations during the baseline period and found good agreement (Supporting Information Text, Figure S4a). TROPOMI's correlation with surface-level monitors (Figure S4a) is a dramatic improvement over the correlation of predecessor instruments [Goldberg et al., 2017]. Moreover, the ratios of 24-hour average $NO_2$ to $NO_2$ near the time of satellite overpass are also similar between least- and most-polluted sites (Figure S4b). We note, however, that satellite-derived $NO_2$ tends to underestimate $NO_2$ in highly polluted urban regions on account of satellite footprint resolution [Judd et al., 2019]. This underestimation coupled with the fact that marginalized communities tend to live closer to potent $NO_2$ sources such as highways (Figure 3) that cannot be resolved given TROPOMI's resolution suggests that our current methodology may underestimate the magnitude of disparities and lockdown-related changes.

Our results are neither an artifact of how we defined demographic subgroups or the time period over which we characterize disparities, although the precise absolute $NO_2$ levels and magnitude of disparities change with the start dates and length of the periods (Figure S5) and how population subgroups are defined (Figure S3). With that said, the length of our baseline and lockdown periods allows spatial heterogeneities to be properly captured when oversampling as well as averages over meteorological variations associated with favorable or unfavorable conditions for $NO_2$ pollution [Goldberg et al., 2020]. We acknowledge that while meteorological and seasonal factors are important factors that could impact our results, they are unlikely to vary in such a way as to be skewed towards certain demographic groups or over the spatial scales of the MSAs focused on throughout this study.

We encourage future work using surface-level $NO_2$ concentrations to better understand exposure across demographic subgroups during lockdowns. Current surface-level observational networks are inadequate for doing so due to their sparse and uneven distribution [Lamsal et al., 2015], but surface concentrations of $NO_2$ inferred using land-use regression models [Novotny et al., 2011] or chemical transport models [Geddes et al., 2016, Cooper et al., 2020] may prove useful. Future

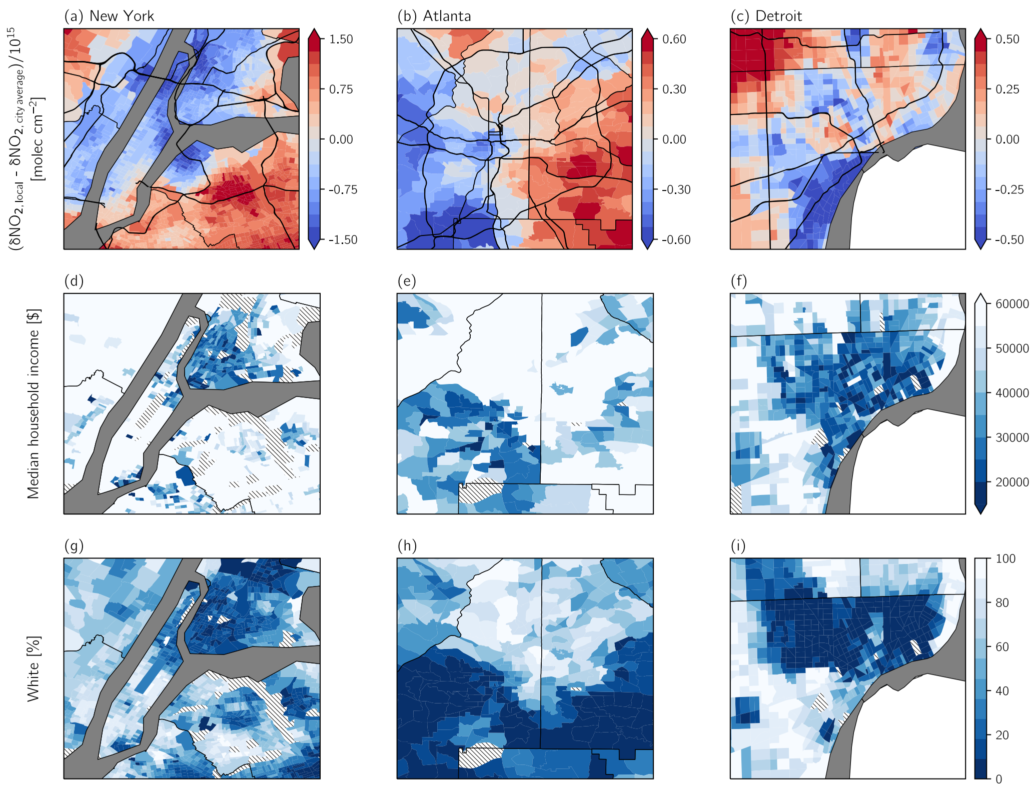


Figure 4. **Case studies of lockdown $NO_2$ drops, income, and race for (left column) New York, (middle) Atlanta, and (right) Detroit.** (a-c) $\Delta$ $NO_{2,\,\mathrm{local}}$ is calculated from oversampled TROPOMI data as the difference between $\Delta$ $NO_2$ and the city average $\Delta$ $NO_2$ to highlight neighborhoods with larger drops (i.e., negative values) and smaller drops (i.e., positive values) compared with the city-averaged drops. Primary roads are shown in thick black lines. (d-f) Median household income and (g-i) percentage of the population that is white. Tracts in (d-i) that are employment centers, airports, parks, or forests and therefore report no demographic data are denoted with hatching.

work might also examine how lockdown-related changes in other air pollutants such as ozone and particulate matter, whose changes during lockdowns do not exhibit the same spatial patterns as $NO_2$ [Chang et al., 2020, Shi and Brasseur, 2020, Venter et al., 2020], impact disparities.

## 6. Conclusions

This study provides a unique, nationwide look at air pollution disparities in the U.S., leveraging the extraordinary confluence of unparalleled changes in human activity during COVID-19 lockdowns and unmatched spatial coverage and resolution of air quality surveillance from the TROPOMI satellite instrument. Lockdowns decreased tropospheric column abundances of $NO_2$ across the vast majority of urban areas. However, drops in $NO_2$ pollution were uneven within these urban areas and largely benefitted communities with a high proportion of racial and ethnic minorities and lower educational attainment and income. Our results reveal that, despite the improvements in $NO_2$ pollution during lockdowns, racial, ethnic, and socioeconomic $NO_2$ disparities persisted, and marginalized communities continued to face higher levels of $NO_2$ during the lockdowns than marginalized communities experienced prior to the pandemic. As traffic emissions represent a major source of $NO_2$ variability, the proximity of marginalized neighborhoods to a high density of major roadways is likely the key determinant in explaining lockdown-related drops in $NO_2$ pollution.

While emissions from passenger vehicle traffic precipitously declined during COVID-19 lockdowns [Parker et al., 2020], there are other potent air pollution sources, such as power generation, heavy-duty trucking, and industry, that were less affected by the COVID-19 pandemic [Kroll et al., 2020]. These other sources are predominately located in marginalized areas [Demetillo et al., 2020, Shah et al., 2020] and likely contribute to the $NO_2$ disparities detailed herein. Nevertheless, our finding that even the $\sim 50\%$ drop in passenger vehicle emissions [Quéré et al., 2020] did not reduce $NO_2$ levels among the most marginalized urban census tracts to the levels experienced by the least marginalized tracts before the pandemic indicates that profound changes are needed to address disparities in $NO_2$ pollution in the U.S. Policies aimed at reducing emissions from passenger vehicle traffic (e.g., mode shifting to public transportation and active transportation, widespread use of electric vehicles) would broadly reduce $NO_2$ levels, but the COVID-19 pandemic lockdowns demonstrated that targeting the passenger vehicle sector alone is unlikely to eliminate $NO_2$ disparities. For this reason, policy strategies that reduce inequality in exposure while maximizing health benefits [Levy et al., 2007] and target a variety of sectors are urgently needed.

## 7. Materials and Methods

7.1. **Remotely-sensed $NO_2$.** We obtain retrievals of the tropospheric $NO_2$ column from the Tropospheric Monitoring Instrument (TROPOMI) aboard the Sentinel-5 Precursor (S5P) satellite. S5P is a nadir-viewing satellite in a sun-synchronous, low-earth orbit that achieves near-global daily coverage with a local overpass time of $\sim$ 1330 hours [Veefkind et al., 2012]. TROPOMI provides $NO_2$ measurements at an unprecedented spatial resolution of $5 \times 3.5$ km$^2$ ($7 \times 3.5$ km$^2$ prior to 6 August

2019) [van Geffen et al., 2020]. We use Level 2 data and only consider pixels with a quality assurance value $> 0.75$. The change in satellite resolution occurring in August 2019 as well as intrinsic limitations stemming from the retrieval process and satellite footprint likely lead to an underestimation of $NO_2$ levels in urban areas and the $NO_2$ change during lockdowns [Bechle et al., 2013, Judd et al., 2019]. TROPOMI data are thereafter oversampled by regridding to a standard grid with a resolution of $0.01°$ latitude $\times$ $0.01°$ longitude ($\sim$ 1 km $\times$1 km) and averaged over two time periods: a baseline period (13 March-13 June 2019) and a lockdown period (13 March-13 June 2020). Regridded data are publicly available at Figshare (`www.figshare.com/s/75a00608f3faedc4bca7`).

Comparing the same time period across different years is commonplace in satellite studies investigating changes in $NO_x$ and other trace gases, and averaging over three month timeframes smooths natural $NO_2$ variations that arise from differences in meteorology and sun angle, which are especially relevant during boreal spring [Goldberg et al., 2020]. This temporal averaging also removes part of the random error in the TROPOMI single-pixel uncertainties, which can be 40-60% of the tropospheric column abundances [Bauwens et al., 2020].

7.2. **Socio-demographic Data.** Demographic information is derived from the American Community Survey (ACS) conducted by the U.S. Census Bureau and maintained by the National Historical Geographic Information System [Manson et al., 2019]. Data are publicly available at `www.nhgis.org`. We extract 2014-2018 5-year estimates on race, Hispanic or Latino origin (henceforth "ethnicity"), educational attainment, median household income, and vehicle availability for the 72,538 census tracts in the contiguous U.S. To minimize the number of different categorical variables presented in this study, we combine racial groups into three categories: white, Black (includes Black and African American), and Other (includes American Indian or Alaska Native, Asian, Native Hawaiian or Other Pacific Islander, two or more races, and some other race). Similarly, we form three different levels for educational attainment: high school (includes no high school diploma, regular high school diploma, and GED or alternative credentials), college (includes some college without a degree, Associate's degree, and Bachelor's degree), and graduate (includes Master's degree, Professional school degree, and Doctorate degree).

7.3. **Methods.** We harmonize the regridded TROPOMI $NO_2$ measurements with tract-level ACS demographics by determining the geographic boundaries of each tract and thereafter calculating a simple arithmetic average over all TROPOMI grid cells within the tract for the baseline and lockdown periods. Approximately 8% of tracts lack a co-located TROPOMI grid cell due to their small size or irregular geometry, and we employ inverse distance weighting interpolation to calculate the $NO_2$ levels at the centroid of these small tracts using the 8 neighboring grid cells. Tracts are classified as either rural or urban based on the census-designed rurality level from the last decadal census in 2010. Urban census tracts lie within the boundaries of an incorporated or census-designed place with $> 2500$ residents, and rural tracts are located outside these boundaries. Therefore, suburban areas on the periphery of cities with $> 2500$ residents are classified as "urban" in this study. We further stratify the tracts into metropolitan-level subsets for the 15 largest MSAs in the U.S.: New York City-Newark-Jersey City, NY-NJ-PA; Los Angeles-Long Beach-Anaheim, CA; Chicago-Naperville-Elgin, IL-IN-WI; Dallas-Fort Worth-Arlington, TX; Houston-The Woodlands-Sugar Land, TX; Washington-Arlington-Alexandria, DC-VA-MD-WV; Miami-Fort Lauderdale-Pompano Beach, FL; Philadelphia-Camden-Wilmington, PA-NJ-DE-MD; Atlanta-Sandy Springs-Alpharetta, GA; Phoenix-Mesa-Chandler, AZ; Boston-Cambridge-Newton, MA-NH; San Francisco-Oakland-Berkeley, CA; Riverside-San Bernardino-Ontario, CA; Detroit-Warren-Dearborn, MI; and Seattle-Tacoma-Bellevue, WA. For brevity we refer to these MSAs by their colloquial names (e.g., Los Angeles, rather than Los Angeles-Long Beach-Anaheim, CA) when discussing them.

We calculate the density of nearby primary roadways for each census tract as a proxy for exposure to traffic-related $NO_2$ pollution. Primary roads are generally divided, limited-access highways within the Interstate Highway System or under state management, and their locations are determined from the U.S. Census Bureau's TIGER/Line geospatial database. Specifically, we determine density as the number of primary road segments within 1 km of a tract's centroid. We choose 1 km as our threshold for what constitutes as "nearby," as $NO_2$ concentrations decrease up to $\sim 50\%$ within $0.5 - 2$ km from major roadways [Novotny et al., 2011, Demetillo et al., 2020], and we note that our findings are robust when considering all primary roads within 2 km (not shown). Other means of quantifying traffic exist (e.g., length of roadway within a specified distance, traffic within buffer zones, sum of distance traveled) [Pratt et al., 2013], but our approach allows for consistent use of geospatial data from the U.S. Census Bureau.

We partition census tracts by extreme values of their change in $NO_2$ ($\Delta$ $NO_2$) or demographic variables using the first decile (0-10th percentile) and tenth decile (90-100th percentile). This partitioning is done individually for different conglomerations or MSAs rather than defining nationwide percentiles to account for urban-rural gradients or differences among MSAs. As examples, tracts classified as "Most white" or "Highest income" have a white population fraction or median household income which falls in the tenth decile. Likewise, $\Delta$ $NO_2$ in tracts with the "Largest drops" (i.e., the largest decrease in $NO_2$ during lockdowns) falls in the first decile. Our results are not sensitive to the use of the first and tenth deciles, and we have tested the upper and lower vigintiles, quintiles, and quartiles and obtain similar results (Figure S3). The use of percentiles rather than absolute thresholds yields a consistent sample size for the upper and lower extrema and also avoids defining absolute thresholds for different variables.

We applied the two-sample Kolmogorov-Smirnov (KS) test to determine whether distributions of demographic variables for the largest and smallest $NO_2$ drops (Figure 1c-h) and tract-averaged $NO_2$ for the upper and lower extrema of demographic variables (Figure 2) are drawn from the same distribution (Figure S6). If the $p$-value corresponding to the KS test statistic is less than $\alpha = 0.05$, we declare that there are significant differences in the distributions. We also assess whether the $NO_2$ disparities shown in Figure 2 undergo significant changes between the baseline and lockdown periods using a two-sample z-test. To meet the normality assumption of the z-test, we log-transform the skewed $NO_2$ distributions prior to computing the test statistic. Changes in baseline versus lockdown disparities are classified as significant when the absolute value of the test statistic is larger than 1.96, the critical value for a 95% level of confidence ($p < 0.05$). We note that this approach to assess the significance of changes in disparities agrees well with other methods, such as examining whether 95% confidence levels of the baseline and lockdown disparities overlap (compare Figures 2 and S2)

The start date of the baseline and lockdowns periods used in this study (13 March) corresponds to the date of national emergency declaration in the U.S. and the beginning of a pronounced decrease in mobility patterns in 2020 [Badr et al., 2020]. We test whether the overall racial, ethnic, income, and educational disparities hold for other periods and find that the disparities among different demographic subgroups persist regardless of the start date or length of the baseline period (Figure S5). We are inherently limited by the short TROPOMI data record, and interannual variability could play a role in modulating the magnitude of disparities in $NO_2$ levels. Testing this possibility is important as more TROPOMI data become available.

## 8. Acknowledgement

Research reported in the publication was supported by NASA under award numbers 80NSSC19K0193 and 80NSSC20K1122. Regridded TROPOMI data used in this study are freely available on Figshare (`www.figshare.com/s/75a00608f3faedc4bca7`), and ACS demographic data are available at `www.nhgis.org`. The authors would like to thank the Netherlands Space Office and European Space Agency for their support of TROPOMI products.

## References

[Achakulwisut et al., 2019] Achakulwisut, P., Brauer, M., Hystad, P., and Anenberg, S. C. (2019). Global, national, and urban burdens of paediatric asthma incidence attributable to ambient $NO_2$ pollution: estimates from global datasets. *The Lancet Planetary Health*, 3(4):e166–e178.

[Anenberg et al., 2018] Anenberg, S. C., Henze, D. K., Tinney, V., Kinney, P. L., Raich, W., Fann, N., Malley, C. S., Roman, H., Lamsal, L., Duncan, B., Martin, R. V., van Donkelaar, A., Brauer, M., Doherty, R., Jonson, J. E., Davila, Y., Sudo, K., and Kuylenstierna, J. C. (2018). Estimates of the global burden of ambient $PM_{2.5}$, ozone, and $NO_2$ on asthma incidence and emergency room visits. *Environmental Health Perspectives*, 126(10):107004.

[Badr et al., 2020] Badr, H. S., Du, H., Marshall, M., Dong, E., Squire, M. M., and Gardner, L. M. (2020). Association between mobility patterns and COVID-19 transmission in the USA: a mathematical modelling study. *The Lancet Infectious Diseases*.

[Bauwens et al., 2020] Bauwens, M., Compernolle, S., Stavrakou, T., Müller, J.-F., Gent, J., Eskes, H., Levelt, P. F., A, R., Veefkind, J. P., Vlietinck, J., Yu, H., and Zehner, C. (2020). Impact of coronavirus outbreak on $NO_2$ pollution assessed using TROPOMI and OMI observations. *Geophysical Research Letters*, 47(11).

[Bechle et al., 2013] Bechle, M. J., Millet, D. B., and Marshall, J. D. (2013). Remote sensing of exposure to $NO_2$: Satellite versus ground-based measurement in a large urban area. *Atmospheric Environment*, 69:345–353.

[Bell and Ebisu, 2012] Bell, M. L. and Ebisu, K. (2012). Environmental inequality in exposures to airborne particulate matter components in the United States. *Environmental Health Perspectives*, 120(12):1699–1704.

[Boehmer et al., 2013] Boehmer, T. K., Foster, S. L., Henry, J. R., Woghiren-Akinnifesi, E. L., and Yip, F. Y. (2013). Residential proximity to major highways - United States, 2010. *Morbidity and Mortality Weekly Report*, 62(3):46–50.

[Chang et al., 2020] Chang, Y., Huang, R.-J., Ge, X., Huang, X., Hu, J., Duan, Y., Zou, Z., Liu, X., and Lehmann, M. F. (2020). Puzzling haze events in China during the coronavirus (COVID-19) shutdown. *Geophysical Research Letters*, 47(12).

[Chauhan et al., 2003] Chauhan, A., Inskip, H. M., Linaker, C. H., Smith, S., Schreiber, J., Johnston, S. L., and Holgate, S. T. (2003). Personal exposure to nitrogen dioxide ($NO_2$) and the severity of virus-induced asthma in children. *The Lancet*, 361(9373):1939–1944.

[Clark et al., 2014] Clark, L. P., Millet, D. B., and Marshall, J. D. (2014). National patterns in environmental injustice and inequality: Outdoor $NO_2$ air pollution in the United States. *PLoS ONE*, 9(4):e94431.

[Clark et al., 2017] Clark, L. P., Millet, D. B., and Marshall, J. D. (2017). Changes in transportation-related air pollution exposures by race-ethnicity and socioeconomic status: outdoor nitrogen dioxide in the United States in 2000 and 2010. *Environmental Health Perspectives*, 125(9):097012.

[Colmer et al., 2020] Colmer, J., Hardman, I., Shimshack, J., and Voorheis, J. (2020). Disparities in $PM_{2.5}$ air pollution in the United States. *Science*, 369(6503):575–578.

[Cooper et al., 2020] Cooper, M. J., Martin, R. V., McLinden, C. A., and Brook, J. R. (2020). Inferring ground-level nitrogen dioxide concentrations at fine spatial resolution applied to the TROPOMI satellite instrument. *Environmental Research Letters*, 15(10):104013.

[Demetillo et al., 2020] Demetillo, M. A. G., Navarro, A., Knowles, K. K., Fields, K. P., Geddes, J. A., Nowlan, C. R., Janz, S. J., Judd, L. M., Al-Saadi, J., Sun, K., McDonald, B. C., Diskin,

G. S., and Pusede, S. E. (2020). Observing nitrogen dioxide air pollution inequality using high-spatial-resolution remote sensing measurements in houston, texas. *Environmental Science & Technology*, 54(16):9882–9895.

[Diffenbaugh et al., 2020] Diffenbaugh, N. S., Field, C. B., Appel, E. A., Azevedo, I. L., Baldocchi, D. D., Burke, M., Burney, J. A., Ciais, P., Davis, S. J., Fiore, A. M., Fletcher, S. M., Hertel, T. W., Horton, D. E., Hsiang, S. M., Jackson, R. B., Jin, X., Levi, M., Lobell, D. B., McKinley, G. A., Moore, F. C., Montgomery, A., Nadeau, K. C., Pataki, D. E., Randerson, J. T., Reichstein, M., Schnell, J. L., Seneviratne, S. I., Singh, D., Steiner, A. L., and Wong-Parodi, G. (2020). The COVID-19 lockdowns: A window into the earth system. *Nature Reviews Earth & Environment*, 1(9):470–481.

[Ding et al., 2020] Ding, J., van der A, R. J., Eskes, H. J., Mijling, B., Stavrakou, T., van Geffen, J. H. G. M., and Veefkind, J. P. (2020). $NO_x$ emissions reduction and rebound in China due to the COVID-19 crisis. *Geophys. Res. Lett.*, 47(19):e2020GL089912.

[Geddes et al., 2016] Geddes, J. A., Martin, R. V., Boys, B. L., and van Donkelaar, A. (2016). Long-term trends worldwide in ambient $NO_2$ concentrations inferred from satellite observations. *Environmental Health Perspectives*, 124(3):281–289.

[Goldberg et al., 2021] Goldberg, D. L., Anenberg, S., Kerr, G. H., Mohegh, A., Lu, Z., and Streets, D. G. (2021). TROPOMI $NO_2$ in the United States: A detailed look at the annual averages, weekly cycles, effects of temperature, and correlation with surface $NO_2$ concentrations. *https://doi.org/10.1002/essoar.10503422.1*.

[Goldberg et al., 2020] Goldberg, D. L., Anenberg, S. C., Griffin, D., McLinden, C. A., Lu, Z., and Streets, D. G. (2020). Disentangling the impact of the COVID-19 lockdowns on urban $NO_2$ from natural variability. *Geophysical Research Letters*, 47(17).

[Goldberg et al., 2017] Goldberg, D. L., Lamsal, L. N., Loughner, C. P., Swartz, W. H., Lu, Z., and Streets, D. G. (2017). A high-resolution and observationally constrained OMI $NO_2$ satellite retrieval. *Atmospheric Chemistry and Physics*, 17(18):11403–11421.

[Goldberg et al., 2019] Goldberg, D. L., Lu, Z., Streets, D. G., de Foy, B., Griffin, D., McLinden, C. A., Lamsal, L. N., Krotkov, N. A., and Eskes, H. (2019). Enhanced capabilities of TROPOMI $NO_2$: Estimating $NO_x$ from North American cities and power plants. *Environmental Science & Technology*, 53(21):12594–12601.

[Hajat et al., 2013] Hajat, A., Diez-Roux, A. V., Adar, S. D., Auchincloss, A. H., Lovasi, G. S., O'Neill, M. S., Sheppard, L., and Kaufman, J. D. (2013). Air pollution and individual and neighborhood socioeconomic status: Evidence from the multi-ethnic study of atherosclerosis (MESA). *Environmental Health Perspectives*, 121(11-12):1325–1333.

[Hajat et al., 2015] Hajat, A., Hsia, C., and O'Neill, M. S. (2015). Socioeconomic disparities and air pollution exposure: a global review. *Current Environmental Health Reports*, 2(4):440–450.

[Hansel et al., 2015] Hansel, N. N., McCormack, M. C., and Kim, V. (2015). The effects of air pollution and temperature on COPD. *COPD: Journal of Chronic Obstructive Pulmonary Disease*, 13(3):372–379.

[He et al., 2020] He, G., Pan, Y., and Tanaka, T. (2020). The short-term impacts of COVID-19 lockdown on urban air pollution in China. *Nature Sustainability.*

[Jerrett et al., 2013] Jerrett, M., Burnett, R. T., Beckerman, B. S., Turner, M. C., Krewski, D., Thurston, G., Martin, R. V., van Donkelaar, A., Hughes, E., Shi, Y., Gapstur, S. M., Thun, M. J., and Pope, C. A. (2013). Spatial analysis of air pollution and mortality in California. *American Journal of Respiratory and Critical Care Medicine*, 188(5):593–599.

[Judd et al., 2019] Judd, L. M., Al-Saadi, J. A., Janz, S. J., Kowalewski, M. G., Pierce, R. B., Szykman, J. J., Valin, L. C., Swap, R., Cede, A., Mueller, M., Tiefengraber, M., Abuhassen, N., and Williams, D. (2019). Evaluating the impact of spatial resolution on tropospheric

$NO_2$ column comparisons within urban areas using high-resolution airborne data. *Atmospheric Measurement Techniques*, 12:6091–6111.

[Kroll et al., 2020] Kroll, J. H., Heald, C. L., Cappa, C. D., Farmer, D. K., Fry, J. L., Murphy, J. G., and Steiner, A. L. (2020). The complex chemical effects of COVID-19 shutdowns on air quality. *Nature Chemistry*, 12:777–779.

[Krotkov et al., 2016] Krotkov, N. A., McLinden, C. A., Li, C., Lamsal, L. N., Celarier, E. A., Marchenko, S. V., Swartz, W. H., Bucsela, E. J., Joiner, J., Duncan, B. N., Boersma, K. F., Veefkind, J. P., Levelt, P. F., Fioletov, V. E., Dickerson, R. R., He, H., Lu, Z., and Streets, D. G. (2016). Aura OMI observations of regional $SO_2$ and $NO_2$ pollution changes from 2005 to 2015. *Atmos. Chem. Phys.*, 16(9):4605–4629.

[Lamsal et al., 2015] Lamsal, L. N., Duncan, B. N., Yoshida, Y., Krotkov, N. A., Pickering, K. E., Streets, D. G., and Lu, Z. (2015). U.S. $NO_2$ trends (2005-2013): EPA Air Quality System (AQS) data versus improved observations from the Ozone Monitoring Instrument (OMI). *Atmospheric Environment*, 110:130–143.

[Landrigan et al., 2018] Landrigan, P. J., Fuller, R., Acosta, N. J. R., Adeyi, O., Arnold, R., Basu, N. N., Baldé, A. B., Bertollini, R., Bose-O'Reilly, S., Boufford, J. I., Breysse, P. N., Chiles, T., Mahidol, C., Coll-Seck, A. M., Cropper, M. L., Fobil, J., Fuster, V., Greenstone, M., Haines, A., Hanrahan, D., Hunter, D., Khare, M., Krupnick, A., Lanphear, B., Lohani, B., Martin, K., Mathiasen, K. V., McTeer, M. A., Murray, C. J. L., Ndahimananjara, J. D., Perera, F., Potočnik, J., Preker, A. S., Ramesh, J., Rockström, J., Salinas, C., Samson, L. D., Sandilya, K., Sly, P. D., Smith, K. R., Steiner, A., Stewart, R. B., Suk, W. A., van Schayck, O. C. P., Yadama, G. N., Yumkella, K., and Zhong, M. (2018). The Lancet Commission on pollution and health. *The Lancet*, 391(10119):462–512.

[Lecocq et al., 2020] Lecocq, T., Hicks, S. P., Noten, K. V., van Wijk, K., Koelemeijer, P., Plaen, R. S. M. D., Massin, F., Hillers, G., Anthony, R. E., Apoloner, M.-T., Arroyo-Solórzano, M., Assink, J. D., Büyükakpınar, P., Cannata, A., Cannavo, F., Carrasco, S., Caudron, C., Chaves, E. J., Cornwell, D. G., Craig, D., den Ouden, O. F. C., Diaz, J., Donner, S., Evangelidis, C. P., Evers, L., Fauville, B., Fernandez, G. A., Giannopoulos, D., Gibbons, S. J., Girona, T., Grecu, B., Grunberg, M., Hetényi, G., Horleston, A., Inza, A., Irving, J. C. E., Jamalreyhani, M., Kafka, A., Koymans, M. R., Labedz, C. R., Larose, E., Lindsey, N. J., McKinnon, M., Megies, T., Miller, M. S., Minarik, W., Moresi, L., Márquez-Ramírez, V. H., Möllhoff, M., Nesbitt, I. M., Niyogi, S., Ojeda, J., Oth, A., Proud, S., Pulli, J., Retailleau, L., Rintamäki, A. E., Satriano, C., Savage, M. K., Shani-Kadmiel, S., Sleeman, R., Sokos, E., Stammler, K., Stott, A. E., Subedi, S., Sorensen, M. B., Taira, T., Tapia, M., Turhan, F., van der Pluijm, B., Vanstone, M., Vergne, J., Vuorinen, T. A. T., Warren, T., Wassermann, J., and Xiao, H. (2020). Global quieting of high-frequency seismic noise due to COVID-19 pandemic lockdown measures. *Science*, 369(6509):1338–1343.

[Levy et al., 2014] Levy, I., Mihele, C., Lu, G., Narayan, J., and Brook, J. R. (2014). Evaluating multipollutant exposure and urban air quality: pollutant interrelationships, neighborhood variability, and nitrogen dioxide as a proxy pollutant. *Environmental Health Perspectives*, 122(1):65–72.

[Levy et al., 2007] Levy, J. I., Wilson, A. M., and Zwack, L. M. (2007). Quantifying the efficiency and equity implications of power plant air pollution control strategies in the United States. *Environmental Health Perspectives*, 115(5):743–750.

[Liang et al., 2020] Liang, D., Shi, L., Zhao, J., Liu, P., Sarnat, J. A., Gao, S., Schwartz, J., Liu, Y., Ebelt, S. T., Scovronick, N., and Chang, H. H. (2020). Urban air pollution may enhance COVID-19 case-fatality and mortality rates in the united states. *The Innovation*, 1(3):100047.

[Manson et al., 2019] Manson, S., Schroeder, J., Riper, D. V., and Ruggles, S. (2019). National historical geographic information system: Version 14.0.

[Martenies et al., 2017] Martenies, S., Milando, C., Williams, G., and Batterman, S. (2017). Disease and health inequalities attributable to air pollutant exposure in Detroit, Michigan. *International Journal of Environmental Research and Public Health*, 14(10):1243.

[Miyazaki et al., 2020] Miyazaki, K., Bowman, K., Sekiya, T., Jiang, Z., Chen, X., Eskes, H., Ru, M., Zhang, Y., and Shindell, D. (2020). Air quality response in China linked to the 2019 novel coronavirus (COVID-19) lockdown. *Geophys. Res. Lett.*, 47(19):e2020GL089252.

[Mohai et al., 2009] Mohai, P., Lantz, P. M., Morenoff, J., House, J. S., and Mero, R. P. (2009). Racial and socioeconomic disparities in residential proximity to polluting industrial facilities: Evidence from the americans' changing lives study. *American Journal of Public Health*, 99(S3):S649–S656.

[Nguyen and Marshall, 2018] Nguyen, N. P. and Marshall, J. D. (2018). Impact, efficiency, inequality, and injustice of urban air pollution: Variability by emission location. *Environmental Research Letters*, 13(2):024002.

[Novotny et al., 2011] Novotny, E. V., Bechle, M. J., Millet, D. B., and Marshall, J. D. (2011). National satellite-based land-use regression: $NO_2$ in the United States. *Environmental Science & Technology*, 45(10):4407–4414.

[Parker et al., 2020] Parker, H. A., Hasheminassab, S., Crounse, J. D., Roehl, C. M., and Wennberg, P. O. (2020). Impacts of traffic reductions associated with COVID-19 on southern California air quality. *Geophys. Res. Lett.*, 47(23):e2020GL090164.

[Patel et al., 2009] Patel, M. M., Chillrud, S. N., Correa, J. C., Feinberg, M., Hazi, Y., Deepti, K., Prakash, S., Ross, J. M., Levy, D., and Kinney, P. L. (2009). Spatial and temporal variations in traffic-related particulate matter at New York City high schools. *Atmospheric Environment*, 43(32):4975–4981.

[Pratt et al., 2013] Pratt, G. C., Parson, K., Shinoda, N., Lindgren, P., Dunlap, S., Yawn, B., Wollan, P., and Johnson, J. (2013). Quantifying traffic exposure. *Journal of Exposure Science & Environmental Epidemiology*, 24(3):290–296.

[Quéré et al., 2020] Quéré, C. L., Jackson, R. B., Jones, M. W., Smith, A. J. P., Abernethy, S., Andrew, R. M., De-Gol, A. J., Willis, D. R., Shan, Y., Canadell, J. G., Friedlingstein, P., Creutzig, F., and Peters, G. P. (2020). Temporary reduction in daily global $CO_2$ emissions during the COVID-19 forced confinement. *Nature Climate Change*, 10(7):647–653.

[Raifman and Raifman, 2020] Raifman, M. A. and Raifman, J. R. (2020). Disparities in the population at risk of severe illness from COVID-19 by race/ethnicity and income. *American Journal of Preventive Medicine*, 59(1):137–139.

[Rose and Mohl, 2012] Rose, M. H. and Mohl, R. A. (2012). *Interstate: Highway Politics and Policy since 1939*. The University of Tennessee Press, Knoxville, 3rd edition.

[Rowangould, 2013] Rowangould, G. M. (2013). A census of the US near-roadway population: Public health and environmental justice considerations. *Transportation Research Part D: Transport and Environment*, 25:59–67.

[Schell et al., 2020] Schell, C. J., Dyson, K., Fuentes, T. L., Roches, S. D., Harris, N. C., Miller, D. S., Woelfle-Erskine, C. A., and Lambert, M. R. (2020). The ecological and evolutionary consequences of systemic racism in urban environments. *Science*, 369(6510):eaay4497.

[Sergi et al., 2020] Sergi, B., Azevedo, I., Davis, S. J., and Muller, N. Z. (2020). Regional and county flows of particulate matter damage in the US. *Environmental Research Letters*, 15(10):104073.

[Shah, 2020] Shah, K. (2020). 'Mostly empty': COVID-19 has nearly shut down world's busiest airport. Accessed October 15, 2020.

[Shah et al., 2020] Shah, R. U., Robinson, E. S., Gu, P., Apte, J. S., Marshall, J. D., Robinson, A. L., and Presto, A. A. (2020). Socio-economic disparities in exposure to urban restaurant emissions are larger than for traffic. *Environmental Research Letters*, 15(11):114039.

[Shi and Brasseur, 2020] Shi, X. and Brasseur, G. P. (2020). The response in air quality to the reduction of Chinese economic activities during the COVID-19 outbreak. *Geophysical Research Letters*, 47(11).

[Stohl et al., 2015] Stohl, A., Aamaas, B., Amann, M., Baker, L. H., Bellouin, N., Berntsen, T. K., Boucher, O., Cherian, R., Collins, W., Daskalakis, N., Dusinska, M., Eckhardt, S., Fuglestvedt, J. S., Harju, M., Heyes, C., Hodnebrog, Ø., Hao, J., Im, U., Kanakidou, M., Klimont, Z., Kupiainen, K., Law, K. S., Lund, M. T., Maas, R., MacIntosh, C. R., Myhre, G., Myriokefalitakis, S., Olivié, D., Quaas, J., Quennehen, B., Raut, J.-C., Rumbold, S. T., Samset, B. H., Schulz, M., Seland, Ø., Shine, K. P., Skeie, R. B., Wang, S., Yttri, K. E., and Zhu, T. (2015). Evaluating the climate and air quality impacts of short-lived pollutants. *Atmospheric Chemistry and Physics*, 15(18):10529–10566.

[Sundvor et al., 2013] Sundvor, I., Balaguer, N. C., Viana, M., Querol, X., Reche, C., Amato, F., Mellios, G., and Guerreiro, C. (2013). Road traffic's contribution to air quality in European cities. Technical report, European Topic Centre for Air Pollution and Climate Change Mitigation.

[Tessum et al., 2019] Tessum, C. W., Apte, J. S., Goodkind, A. L., Muller, N. Z., Mullins, K. A., Paolella, D. A., Polasky, S., Springer, N. P., Thakrar, S. K., Marshall, J. D., and Hill, J. D. (2019). Inequity in consumption of goods and services adds to racial–ethnic disparities in air pollution exposure. *Proceedings of the National Academy of Sciences*, 116(13):6001–6006.

[US Environmental Protection Agency, 2015] US Environmental Protection Agency (2015). 2014 National Emissions Inventory (NEI) data. `https://www.epa.gov/air-emissions-inventories/2014-national-emissions-inventory-nei-data`. Accessed October 15, 2020.

[van Geffen et al., 2020] van Geffen, J., Boersma, K. F., Eskes, H., Sneep, M., ter Linden, M., Zara, M., and Veefkind, J. P. (2020). S5P TROPOMI $NO_2$ slant column retrieval: method, stability, uncertainties and comparisons with OMI. *Atmospheric Measurement Techniques*, 13(3):1315–1335.

[Veefkind et al., 2012] Veefkind, J., Aben, I., McMullan, K., Förster, H., de Vries, J., Otter, G., Claas, J., Eskes, H., de Haan, J., Kleipool, Q., van Weele, M., Hasekamp, O., Hoogeveen, R., Landgraf, J., Snel, R., Tol, P., Ingmann, P., Voors, R., Kruizinga, B., Vink, R., Visser, H., and Levelt, P. (2012). TROPOMI on the ESA Sentinel-5 Precursor: a GMES mission for global observations of the atmospheric composition for climate, air quality and ozone layer applications. *Remote Sensing of Environment*, 120:70–83.

[Venter et al., 2020] Venter, Z. S., Aunan, K., Chowdhury, S., and Lelieveld, J. (2020). COVID-19 lockdowns cause global air pollution declines. *Proceedings of the National Academy of Sciences*, 117(32):18984–18990.

# SUPPORTING INFORMATION FOR "COVID-19 PANDEMIC REVEALS PERSISTENT DISPARITIES IN NITROGEN DIOXIDE POLLUTION"

GAIGE HUNTER KERR[1], DANIEL L. GOLDBERG[1,2], SUSAN C. ANENBERG[1]

[1]*Department of Environmental and Occupational Health, Milken Institute School of Public Health, George Washington University, Washington, DC, 20052 USA,*
[2] *Energy Systems Division, Argonne National Laboratory, Lemont, IL, 60439 USA*

## 1. Remotely-sensed versus surface-level $NO_2$

We compare tropospheric column $NO_2$ from TROPOMI with ground-based observations from the Environmental Protection Agency's Air Quality System (AQS) [US Environmental Protection Agency, nda] to test whether TROPOMI can provide an accurate characterization of differences in surface-level $NO_2$ during the baseline period (13 March - 13 June 2019). There are 439 AQS monitors in the contiguous U.S. with observations during the baseline period, and we average hourly observations over the entire baseline period at each of these sites and compare them with TROPOMI retrievals at the collocated grid cell to each site.

We find that 71 of the 439 monitors are located near (< 20 meters) roads [US Environmental Protection Agency, ndb]. These sites generally have observed surface-level $NO_2$ > 10 ppbv despite relatively low columnar amounts from TROPOMI (Figure S4). We do not expect TROPOMI to capture the large, sharp gradients of $NO_2$ near roadways on account of the differences in scale between the footprint of the satellite and point-based observations. When we consider only AQS monitors that are not located near roads, we find good agreement between these surface-level observations and TROPOMI (Figure 4a). We also find a similar ratio of $NO_2$ averaged over the 24-hour diurnal cycle to $NO_2$ near the time of satellite overpass at sites that are classified as the most and least polluted (Figure 4b). Additional factors such as instrument error (for both TROPOMI and AQS) and clear sky biases may contribute to deviations from a perfect linear relationship between the space-based and surface-level observations [Geddes et al., 2012, Bechle et al., 2013, Judd et al., 2019]; however, the findings of this analysis lend credibility to our reliance on TROPOMI to characterize disparities in $NO_2$ at earth's surface.

*E-mail address*: `gaigekerr@gwu.edu`.

## References

[Bechle et al., 2013] Bechle, M. J., Millet, D. B., and Marshall, J. D. (2013). Remote sensing of exposure to $NO_2$: Satellite versus ground-based measurement in a large urban area. *Atmospheric Environment*, 69:345–353.

[Geddes et al., 2012] Geddes, J. A., Murphy, J. G., O'Brien, J. M., and Celarier, E. A. (2012). Biases in long-term $NO_2$ averages inferred from satellite observations due to cloud selection criteria. *Remote Sensing of the Environment*, 124:210–216.

[Judd et al., 2019] Judd, L. M., Al-Saadi, J. A., Janz, S. J., Kowalewski, M. G., Pierce, R. B., Szykman, J. J., Valin, L. C., Swap, R., Cede, A., Mueller, M., Tiefengraber, M., Abuhassan, N., and Williams, D. (2019). Evaluating the impact of spatial resolution on tropospheric $NO_2$ column comparisons within urban areas using high-resolution airborne data. *Atmospheric Measurement Techniques*, 12(11):6091–6111.

[US Environmental Protection Agency, nda] US Environmental Protection Agency (n.d.a). Air Quality System Data Mart. `https://www.epa.gov/airdata`. Accessed October 21, 2020.

[US Environmental Protection Agency, ndb] US Environmental Protection Agency (n.d.b). Near-road $NO_2$ monitoring. `https://www3.epa.gov/ttnamti1/nearroad.html`. Accessed October 22, 2020.

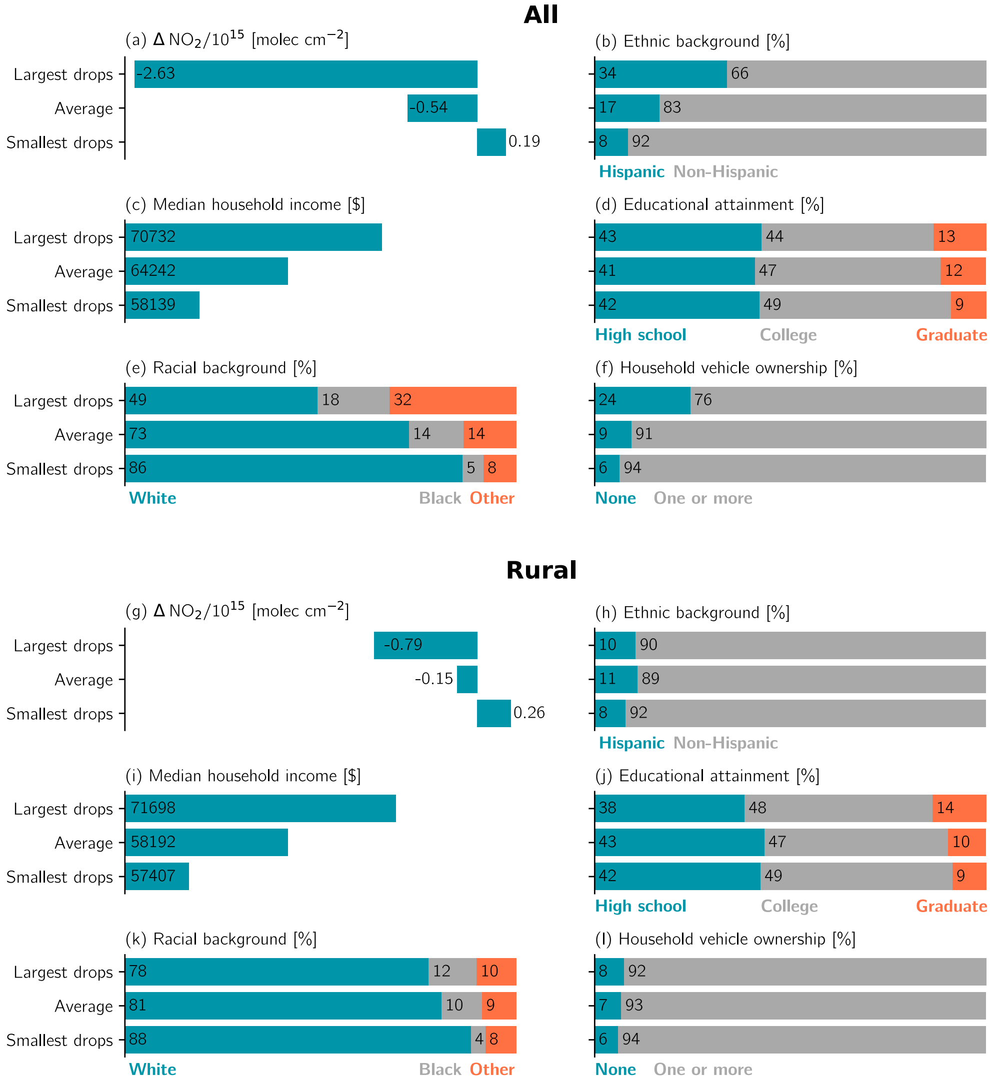


FIGURE 1. Same as Figure 1c-h in the main text but drops and averages are derived from (a-f) all tracts and (g-l) rural tracts.

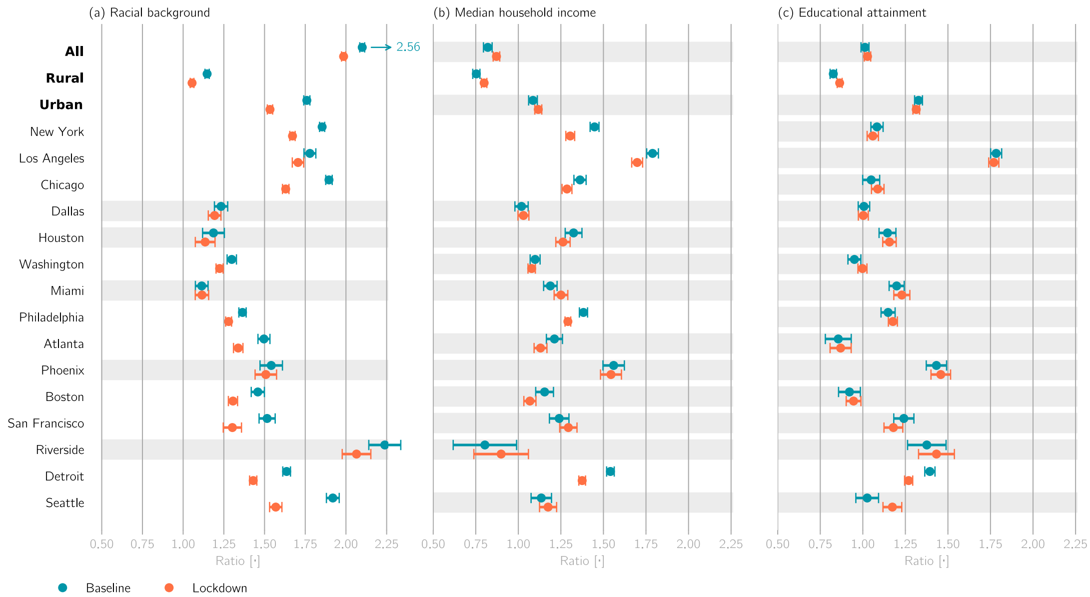


Figure 2. Following Figure 2 in the main text, we calculate the ratio of mean $NO_2$ in the (a) least white to most white, (b) lowest income to highest income, and (c) least educated to most educated census tracts. Horizontal bars indicate the 95% confidence intervals for the mean ratios. Spatial conglomerations or MSAs with confidence intervals that overlap between the baseline and lockdown periods are shaded in grey.

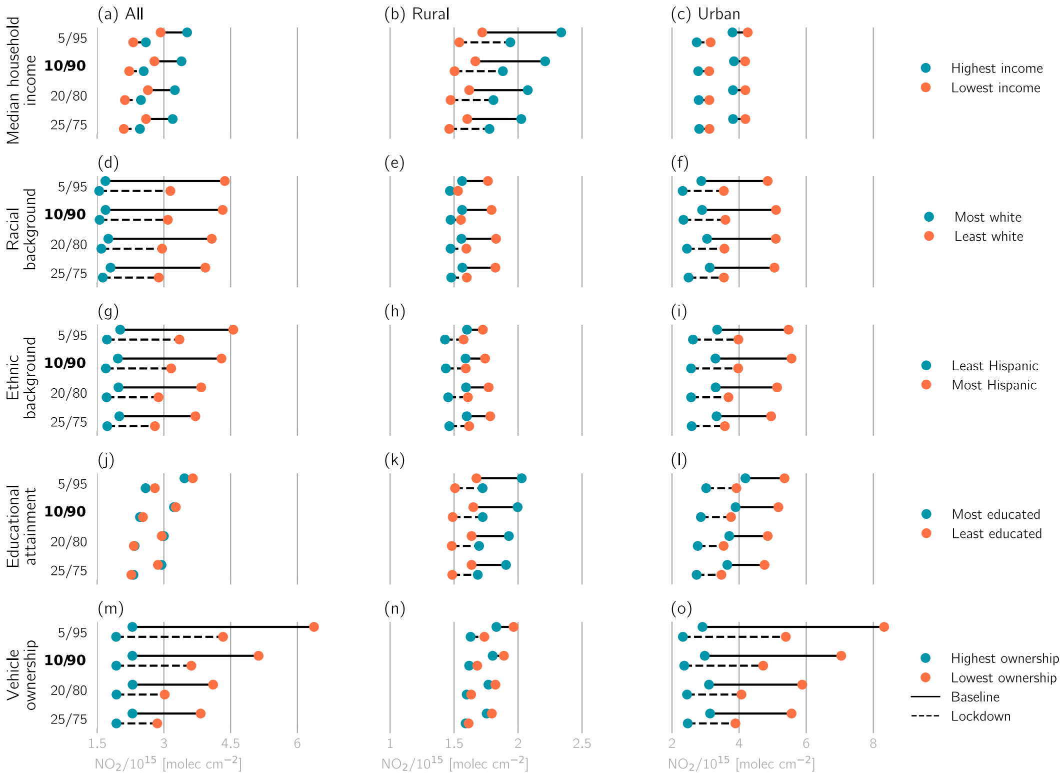


FIGURE 3. **Sensitivity of $NO_2$ disparities to percentiles chosen to constitute extreme values for each demographic variable.** Interpretation follows Figure 2 in the main text, but each pair of bars in individual subplots represents different percentile thresholds, indicated in the subplots' vertical axes. The boldface 10/90 row corresponds to the first and tenth deciles used in the main text.

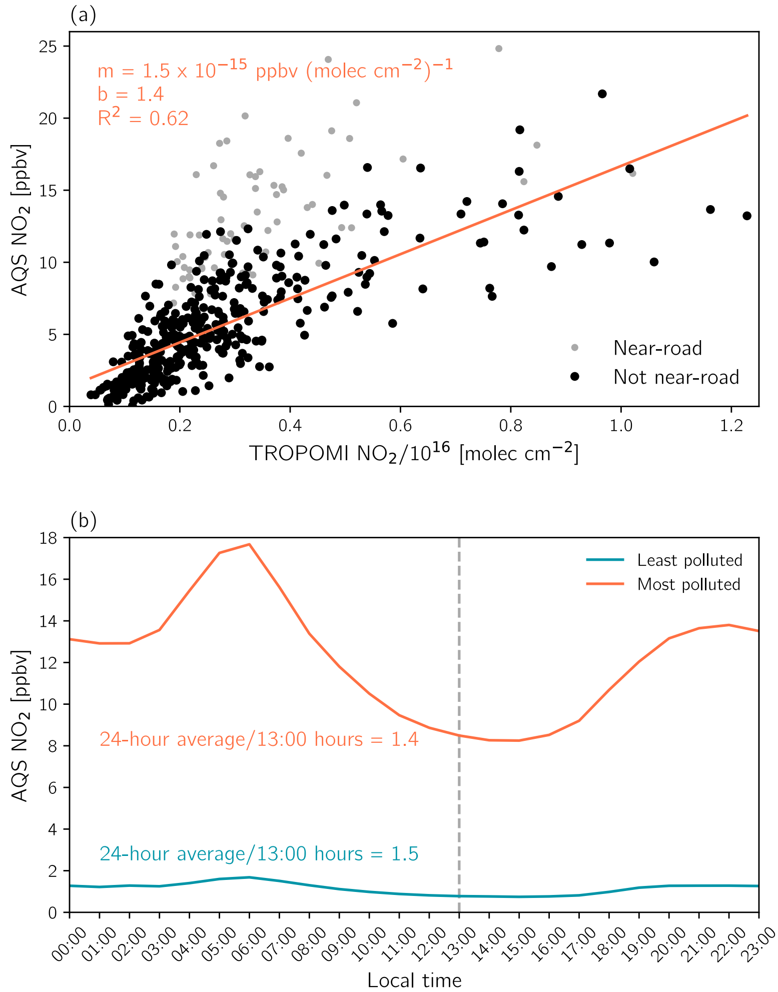


FIGURE 4. (a) Observed $NO_2$ from AQS monitors versus TROPOMI tropospheric $NO_2$ columns averaged over the baseline period (13 March - 13 June 2019). TROPOMI data correspond to the nearest 0.01° latitude × 0.01° longitude grid cell to each AQS monitor. The orange line represents the linear regression fitted only through AQS data not flagged as "near-road" ($<$ 20 meters). The orange text gives the slope (m) and intercept (b) of this linear fit. (b) Observed diurnal cycles of $NO_2$ averaged over the most polluted (AQS monitors where the collocated TROPOMI grid cell $>$ 90th percentile) and least polluted sites (AQS monitors where the collocated TROPOMI grid cell $<$ 10th percentile) during the baseline period. Only sites that are not near-road are considered for these averages. The ratios of 24-hour average $NO_2$ to $NO_2$ at the approximate time of satellite overpass (dashed grey line; $\sim$ 13:00 hours local time) are indicated in the colored text.

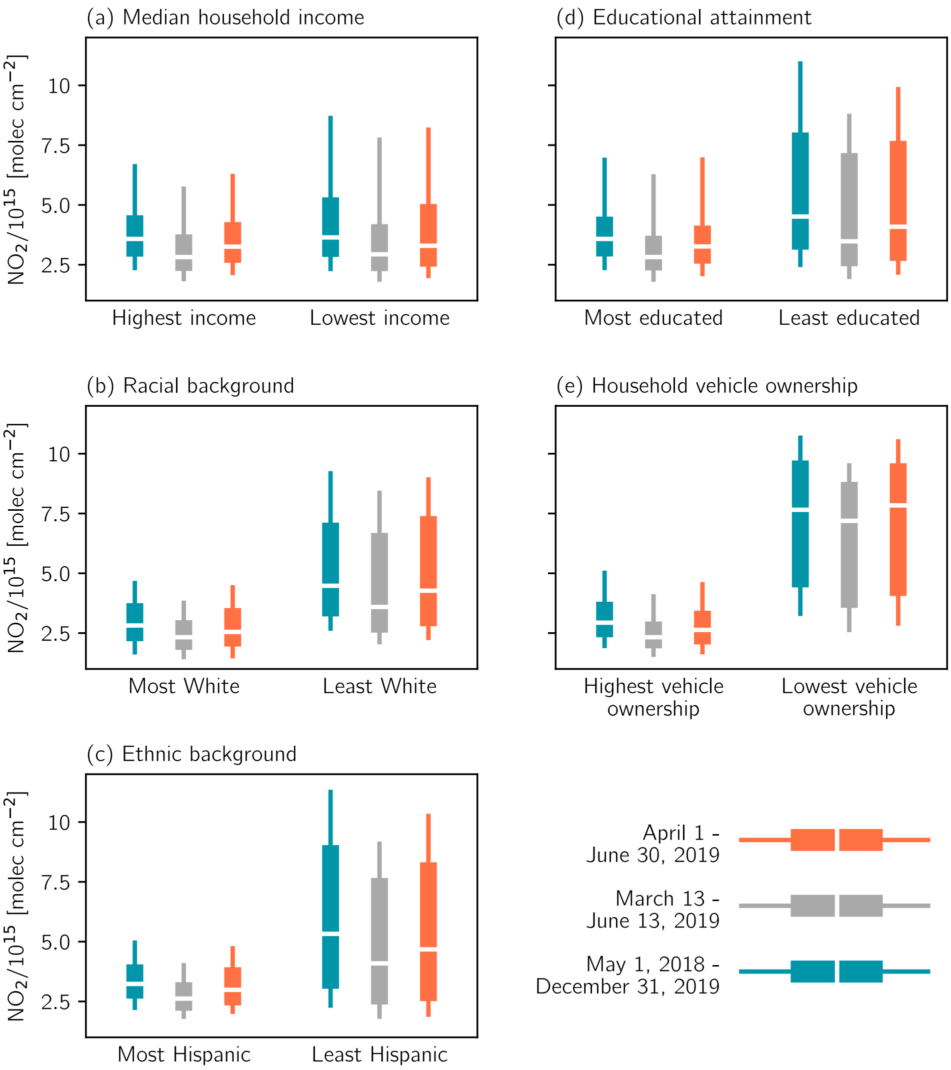


FIGURE 5. **Sensitivity of urban $NO_2$ disparities to the baseline period.** Extreme values of each demographic variable (using the first and tenth deciles) for three different baseline periods: 1 April - 30 June 2019, 13 March - 13 June 2019 (the period used in the main text), and 1 May 2018 - 31 December 2019 (the entire TROPOMI data record). Boxes extend to the lower and upper quartiles of the data, and the median value is indicated with the horizontal white lines. The lower and upper whiskers extend to the 10th and 90th percentiles, respectively.

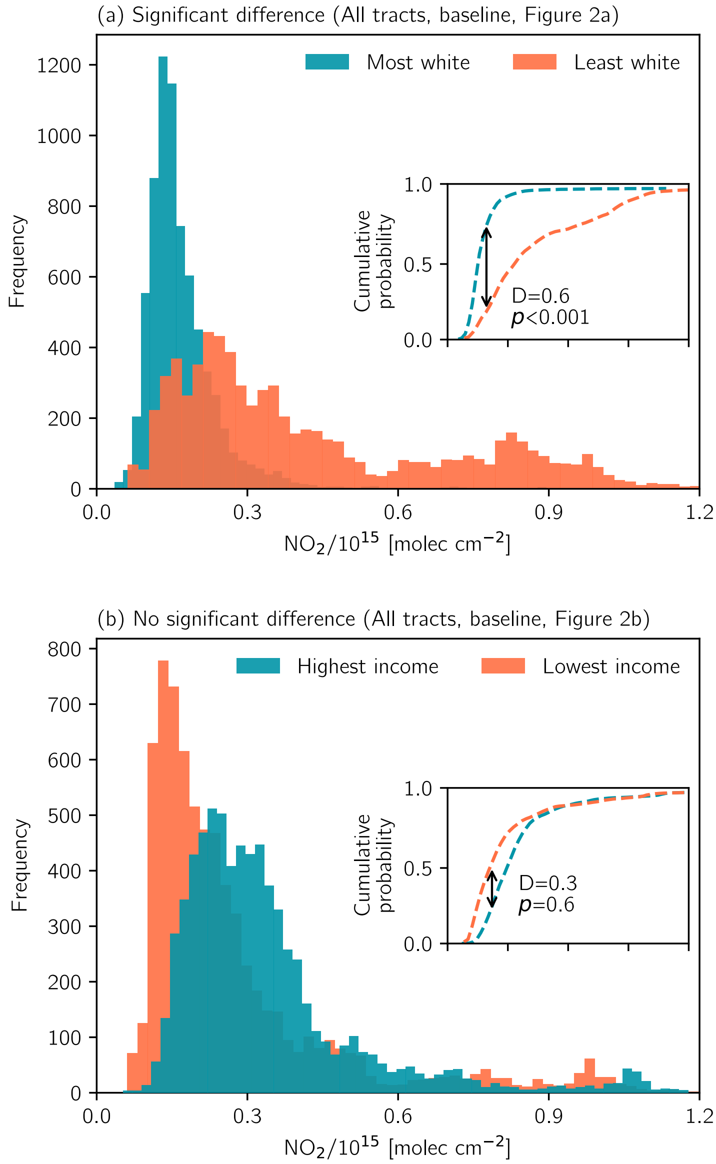


Figure 6. **Illustration of the two-sample Kolmogorov-Smirnov (KS) test used to compare whether $NO_2$ or demographic distributions from different population subgroups are drawn from the same distribution.** $NO_2$ distributions are shown for (a) the most and least white census tracts and (b) the highest and lowest income census tracts (for both urban and rural tracts) during the baseline period. Inset axes in (a)-(b) illustrate the empirical cumulative distribution functions (ECDFs) for each population subgroups' $NO_2$ distribution. The KS test statistic, D, representing the absolute maximum distance between the ECDFs of the two distributions and the associated $p$ values are also indicated in the inset axes. Ticks on the x-axis of the insets are identical to the parent axes. The $p$-value in (a) indicates that the two population subgroups with statistically different $NO_2$ distributions, while the large $p$-value in (b) indicates the difference between the two distributions is not significant at the 95% confidence level.